Journal of Instrumentation

SISSA

OPEN ACCESS

Optimization of the radiation hardness of silicon pixel sensors for high x-ray doses using TCAD simulations

To cite this article: J Schwandt *et al* 2012 *JINST* **7** C01006

View the article online for updates and enhancements.

Related content

- Study of X-ray radiation damage in silicon sensors
  J Zhang, E Fretwurst, R Klanner et al.
- Design of the AGIPD sensor for the European XFEL
  J Schwandt, E Fretwurst, R Klanner et al.
- Investigation of X-ray induced radiation damage at the Si-SiO_2 interface of silicon sensors for the European XFEL
  J Zhang, E Fretwurst, R Klanner et al.

Recent citations

- Simulation of surface radiation defects leakage current SiPM using Synopsys TCAD
  P P Parygin *et al*
- Development of edgeless silicon pixel sensors on p-type substrate for the ATLAS high-luminosity upgrade
  G. Calderini *et al*
- Optimization of radiation hardness and charge collection of edgeless silicon pixel sensors for photon science
  J Zhang *et al*

This content was downloaded from IP address 131.169.4.70 on 28/11/2017 at 11:44

Jinst

PUBLISHED BY IOP PUBLISHING FOR SISSA

RECEIVED: *November 4, 2011*
ACCEPTED: *November 28, 2011*
PUBLISHED: *January 3, 2012*

THE 9th INTERNATIONAL CONFERENCE ON POSITION SENSITIVE DETECTORS,
12–16 SEPTEMBER 2011,
ABERYSTWYTH, U.K.

Optimization of the radiation hardness of silicon pixel sensors for high x-ray doses using TCAD simulations

J. Schwandt,[a,1] **E. Fretwurst,**[a] **R. Klanner,**[a] **I. Pintilie**[a,b] **and J. Zhang**[a]

[a]*Institute for Experimental Physics, University of Hamburg,*
Luruper Chaussee 149, D-22761 Hamburg, Germany
[b]*National Institute of Material Physics,*
P.O.Box MG-7, Bucharest-Magurele, Romania

E-mail: joern.schwandt@desy.de

ABSTRACT: The European X-ray Free Electron Laser (XFEL) will deliver 27000 fully coherent, high brilliance X-ray pulses per second each with a duration below 100 fs. This will allow the recording of diffraction patterns of single molecules and the study of ultra-fast processes. One of the detector systems under development for the XFEL is the Adaptive Gain Integrating Pixel Detector (AGIPD), which consists of a pixel array with readout ASICs bump-bonded to a silicon sensor with pixels of 200×200 μm^2. The particular requirements for the detector are a high dynamic range (0, 1 up to 10^5 12 keV photons/XFEL-pulse), a fast read-out and radiation tolerance up to doses of 1 GGy of 12 keV X-rays for 3 years of operation. At this X-ray energy no bulk damage in silicon is expected. However fixed oxide charges in the SiO_2 layer and interface traps at the Si-SiO_2 interface will build up.

As function of the 12 keV X-ray dose the microscopic defects in test structures and the macroscopic electrical properties of segmented sensors have been investigated. From the test structures the oxide charge density, the density of interface traps and their properties as function of dose have been determined. It is found that both saturate (and even decrease) for doses above a few MGy. For segmented sensors surface damage introduced by the X-rays increases the full depletion voltage, the surface leakage current and the inter-pixel capacitance. In addition an electron accumulation layer forms at the Si-SiO_2 interface which increases with dose and decreases with applied voltage. Using TCAD simulations with the dose dependent damage parameters obtained from the test structures the results of the measurements can be reproduced. This allows the optimization of the sensor design for the XFEL requirements.

KEYWORDS: X-ray detectors; Radiation-hard detectors; Detector modelling and simulations II (electric fields, charge transport, multiplication and induction, pulse formation, electron emission, etc.)

[1]Corresponding author.

© 2012 IOP Publishing Ltd and SISSA

doi:10.1088/1748-0221/7/01/C01006

2012 JINST 7 C01006

Contents

1 **Introduction** 1

2 **Formation of X-ray radiation damage and its influence on p^+-n sensors** 1

3 **Measurement results for X-ray induced radiation damage** 2

4 **TCAD simulations for the AGIPD sensor** 4
- 4.1 Doping profiles 4
- 4.2 Models used in device simulation and scaling from 2D to 3D 6
- 4.3 Simulation results 6

5 **Summary** 9

2012 JINST 7 C01006

1 Introduction

The European X-ray Free Electron Laser (XFEL), currently under construction and planned to be operational in 2015, will increase the peak brilliance of X-rays by 9 orders of magnitude, compared to the third generation storage rings [1, 2]. The XFEL will provide 27000 fully coherent X-ray pulses per second each with a duration below 100 fs and with up to 10^{12} 12 keV photons. These pulses are distributed in bunch trains containing each 2700 pulses separated by 220 ns and a bunch train repetition rate of 10 Hz.

The high dynamic range from 0, 1 up to 10^5 12 keV photons per pixel and the expected radiation dose of up to 1 GGy (SiO_2) for 3 years of operation [2] is a challenge for the design of imaging silicon pixel detectors.

The high density of photons per pulse will create a so called electron-hole plasma which changes the electric field inside the sensor and will influence among others the linearity, point spread function and response time of the detector. As shown in [3], for the reduction of these effects a high operational voltage of the detector is desirable.

The expected radiation dose of up to 1 GGy (SiO_2) is far beyond today's experience. The optimization of sensors for this dose demands a good understanding of the radiation damage caused by X-rays. The aim of this work is to use the relevant parameters for the radiation damage as function of X-ray dose for the simulation of the sensor performance vs. dose, which is needed for the optimization of the sensor design for radiation hardness.

2 Formation of X-ray radiation damage and its influence on p^+-n sensors

For 12 keV photons the main interaction process with Si and SiO_2 is the photoelectric effect. For this photon energy the maximum energy transfer of the secondary electrons to silicon atoms is 0.011 eV, which is far below the threshold energy of 21 eV for bulk damages [4]. Therefore no bulk damage is expected.

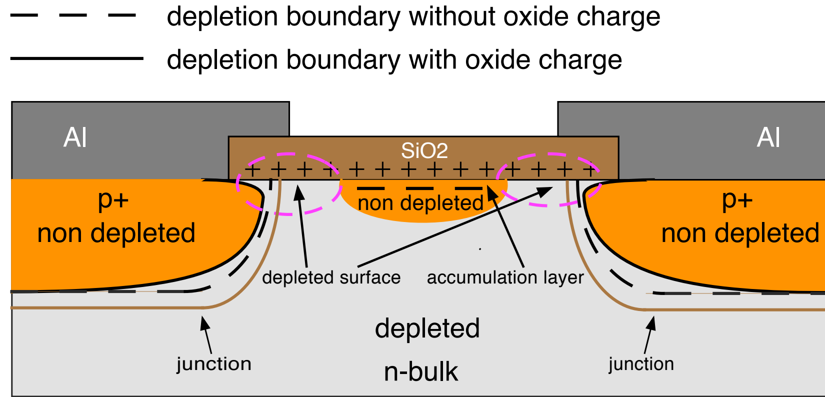

Figure 1. Effects of the oxide charge on a p^+-n sensor. A positive oxide charge bends the depletion boundary and increases the width of the accumulation layer. Thus the width of the depleted region at the Si-SiO_2 interface decreases.

In the SiO_2 the photon-induced damage process is as follow [5]: the secondary electrons generate electron-hole pairs (e-h pairs), where the average energy to produce an e-h pair is 18 eV. Once generated, depending on the electric field, a fraction of the e-h pairs annihilates through recombination. Due to their high mobility the electrons are rapidly swept out of the dielectric. The remaining holes will undergo polaron hopping transport via shallow traps in the SiO_2. A fraction of these holes may be captured by deep traps in the oxide bulk or near the Si-SiO_2 interface, thereby forming fixed positive charges. In addition reactions between holes and hydrogen-containing defects or dopant complexes at the interface can lead to the formation of interface traps, which have energy levels distributed throughout the silicon band gap. The details depend among other things on the oxide thickness, electrical field, dose rate, crystal orientation and fabrication technology.

The impact of the surface damage on a segmented p^+-n sensor is shown schematically in figure 1. Near the junction the positive oxide charge changes the electric field in such a way, that the depletion width along the surface is shorter and the depletion boundary exhibits a stronger curvature compared to the case without oxide charges. This results in a local high electric field and a lower breakdown voltage. In addition, between the junctions below the oxide an electron accumulation layer forms. This accumulation layer prevents a full depletion of the surface and affects the inter-pixel capacitance, the inter-pixel resistance and may cause charge losses.

The effects of the interface traps are twofold. Firstly, depending on the type (donor or acceptor), energy level and Fermi energy they can be positively or negatively charged and thus contribute to the effective oxide charge. Secondly, due to surface recombination at the depleted surface they are responsible for the surface leakage current, which can be parametrized as $I_s = 0.5 q_0 s_0 n_i A_s$ with the elementary charge q_0, the intrinsic carrier density n_i, the depleted surface A_s and the surface recombination velocity $s_0 = \sigma v_{th} N_{it}$, where σ is the capture cross section, v_{th} the thermal velocity of the carriers and N_{it} the interface trap density.

3 Measurement results for X-ray induced radiation damage

From the previous discussion it follows that the relevant parameters are the oxide charge density N_{ox} and the interface trap density distribution. For their experimental determination MOS capacitors

2012 JINST 7 C01006

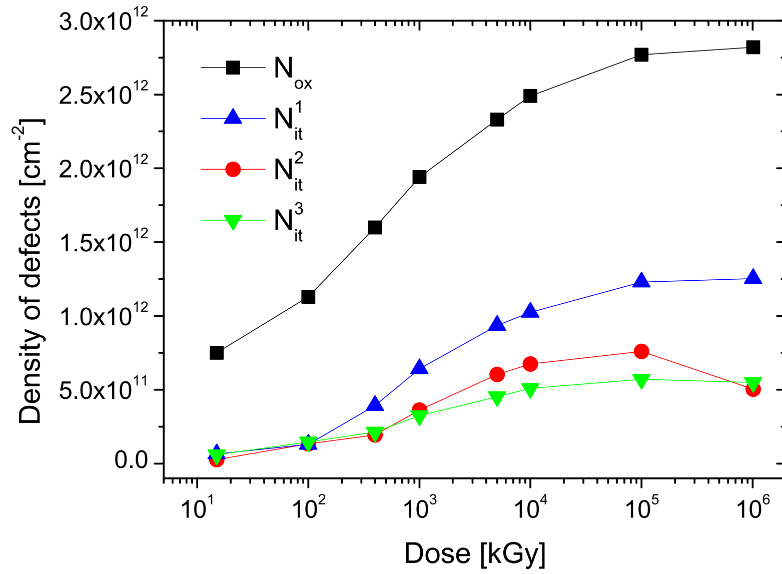

Figure 2. Dose dependence of the fixed oxide charge density N_{ox} and the densities of the three dominant X-ray induced interface traps as function of X-ray irradiation dose after annealing at 80 °C for 10 minutes and crystal orientation <100>.

Table 1. Dose dependence of the fixed oxide charge density N_{ox} and the surface recombination velocity s_0 measured on gate controlled diodes with <111> orientation after annealing at 80 °C for 60 minutes.

Dose [MGy]	0	0.1	1	10	100
N_{ox} [cm^{-2}]	1.0×10^{11}	1.3×10^{12}	2.1×10^{12}	2.8×10^{12}	2.9×10^{12}
s_0 [cm/s]	8	3.5×10^3	7.5×10^3	1.2×10^4	1.1×10^4

and gate controlled diodes fabricated by CiS were irradiated up to 1 GGy with 12 keV X-rays and Thermally Dielectric Relaxation Current (TDRC), Capacitance/Conductance-Voltage (C/G-V) measurements as function of frequency have been performed. Details on the irradiation setup, the test structures and the extraction of the damage parameters can be found in [6] and [7]. Here, only the summary is given: the radiation induced effects can be described by a dose dependent value of the fixed oxide charge density N_{ox} and the densities of three acceptor like interface trap levels $N_{it}^{1,2,3}$. For MOS capacitors with crystal orientation <100> the dose dependences of N_{ox} and of $N_{it}^{1,2,3}$ are shown in figure 2. As function of dose they increase and finally saturate for values above 10 to 100 MGy. The saturation value of N_{ox} is 2.8×10^{12} cm^{-2}. Similar results were obtained for gate controlled diodes with <111> orientation. In the TCAD simulations the damage parameters presented in table 1 were used. The interface trap densities $N_{it}^{1,2,3}$ were not explicitly introduced in the simulation, instead the measured surface recombination velocity s_0 was used. Its value as function of dose was obtained from I/V measurements of gate controlled diodes [8].

2012 JINST 7 C01006

Table 2. AGIPD sensor specifications (V_{fd} full depletion voltage, V_{op} operation voltage, C_{int} inter-pixel capacitance, I_{leak} leakage current).

Parameter	Specification
Thickness	500 μm
Pixel size	200 μm × 200 μm
Type	p^+-n
Resistivity	5 kΩ·cm
V_{fd}	< 200 V
V_{op}	$\geqslant 500$ V
C_{int}	< 0.5 pF
I_{leak}	1 nA/pixel

4 TCAD simulations for the AGIPD sensor

The Adaptive Gain Integrating Pixel Detector (AGIPD) [9] is one of the three large 2D detector projects approved by the European XFEL Company. Based on detector and science simulations [10], studies on plasma effects and technology criteria, the AGIPD collaboration has specified the sensor parameter listed in the table 2.

The parameters which can been optimized in the design of the sensor to fulfill the specifications (see figure 3) are the inter-pixel gap, the metal overhang, the curvature at the implant corners and the guard ring structure. Other parameter like oxide thickness, junction depth and passivation thickness are typically given by the vendors' technology and may only be changed in a limited range or not at all.

To determine the optimum values for above parameters taking into account the surface damage Synopsys TCAD simulations [11] were performed. In a first step the focus was put on the optimization of the gap and the metal overhang. For this 2D simulations were carried out and the resulting currents and capacitances were scaled to 3D. Using 2D simulations, even if the problem of pixels is intrinsically a 3D one, is motivated by the fact, that the inclusion of surface damages requires a very fine mesh at the Si-SiO_2 interface, which requires large amount of computer time and a large direct access memory.

To take the dose dependent effects into account a similar oxide thickness as the one of the test structures was used and the measured values for the fixed oxide charge densities together with the surface recombination velocities given in table 1 were used. For the fixed oxide charge the assumption was made, that the spatial distribution along the Si-SiO_2 interface is uniform. The effect of the interface traps is taken into account only via the surface recombination velocity.

4.1 Doping profiles

As discussed in section 2 the doping profile near the implant edges is essential for the simulation of the effects of surface damages. To get realistic doping profiles 2D process simulations were performed involving the oxide deposition, etching of the implant window, ion implantation and the dopant activation steps. The details are: phosphorous doping of 10^{12} cm^{-3} and <111> orientation for the wafer and boron doses of 10^{15} cm^{-2} to 10^{16} cm^{-2} and energies from 70 keV to 200 keV for the p^+ implantation.

2012 JINST 7 C01006

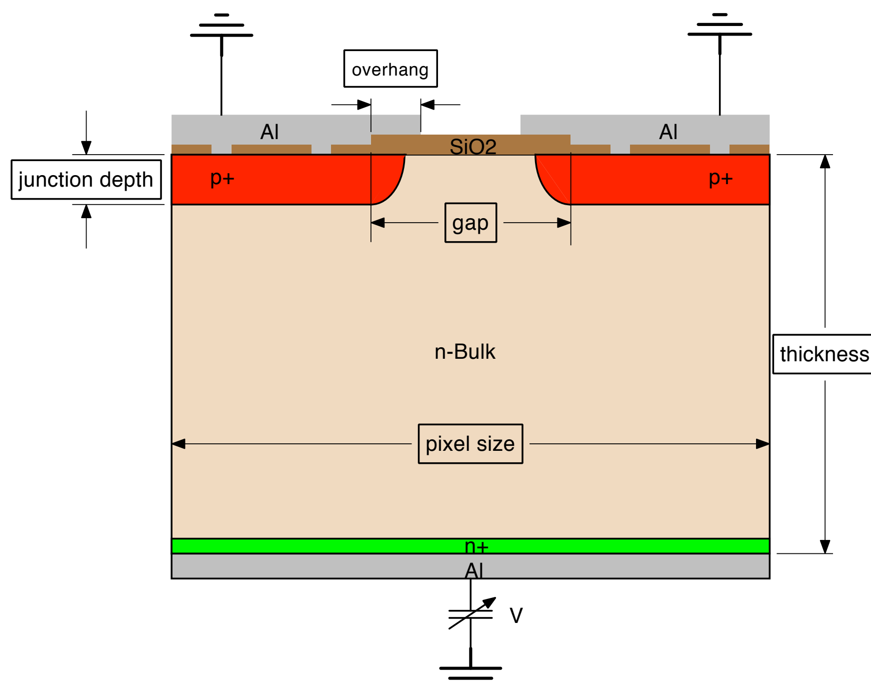

Figure 3. Sketch of sensor region simulated. The parameters optimized as function of the voltage applied between pixel (p^+) and backplane (n^+) in view of radiation hardness are: Al-overhang, gap-size and junction depth.

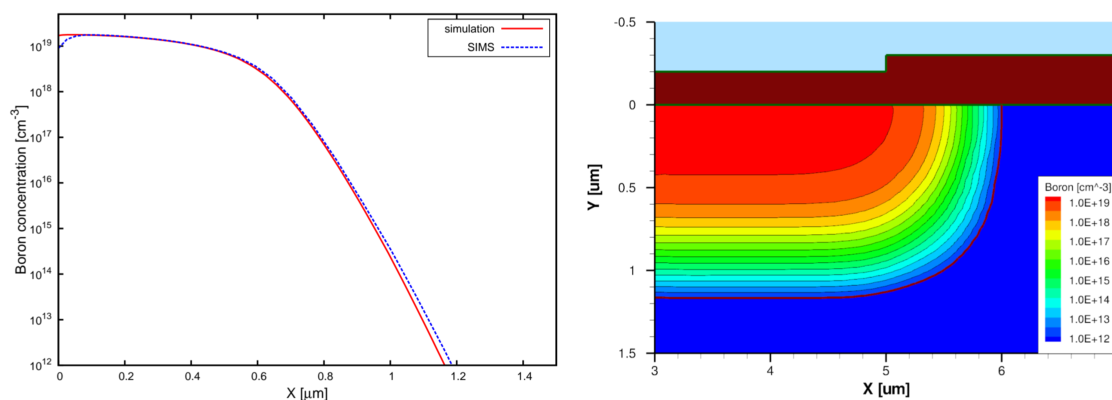

Figure 4. Left: comparison of the simulated boron profile with a parameterization of the SIMS measurement. Right: simulated 2D boron profile.

The simulation was calibrated by comparison of the boron depth profile for the dose of 10^{15} cm^{-2} and the energy of 70 keV with a parameterization of the SIMS measurement for the same process, as shown in the left plot of figure 4. The right plot of figure 4 shows the corresponding 2D boron profile from which one finds a junction depth of 1.2 µm and a lateral extension of 1.0 µm, measured from the edge of the implant. In the following device simulations this doping profile was used and for comparison, the profile from a process which gives a junction depth of 2.4 µm and a lateral extension of 1.95 µm.

2012 JINST 7 C01006

Table 3. Simulated gap and metal overhang values.

gap [µm]	20	30	40
overhang [µm]	0, 2.5, 5	5, 10	0, 2.5, 5, 10

4.2 Models used in device simulation and scaling from 2D to 3D

The geometric model used in the 2D device simulation is shown in figure 3. The simulated pixel size was 200 µm, the sensor thickness 500 µm and the oxide thickness 300 nm. The gap and metal overhang were varied in the range given in table 3.

The device simulations were performed for a temperature of 293 K using the drift-diffusion model with standard models, as implemented in [11], for mobility (with degradation at interfaces), SRH recombination (carrier lifetime 1 ms), band-to-band tunneling and avalanche generation, where the van Overstraeten - de Man model was used. At the top of the SiO_2 Neumann boundary conditions were used.

To scale the 2D results to 3D the following simplifying assumptions were made: for the bulk current, which dominates the current of a non-irradiated sensor, a scaling with the bulk volume was performed. For the surface current, which dominates for irradiated sensors, a scaling with the SiO_2 area was performed. This results in an additional factor 2 compared to the bulk scaling. For the scaling of the 2D simulated inter-strip capacitances $C^{str}_{int,sim}$ analytical expressions for the inter-strip capacitance $C^{str}_{int,theo}$ [13] and for the inter-pixel capacitance $C^{pix}_{int,theo}$ [14], which both neglect the metal overhang, were used and the assumption that the 3D simulated inter-pixel capacitance $C^{pix}_{int,sim}$ is given by

$$C^{pix}_{int,sim} = \frac{C^{str}_{int,sim}}{C^{str}_{int,theo}} \times C^{pix}_{int,theo} \tag{4.1}$$

was made.

4.3 Simulation results

First the results of the dose and voltage dependence of the electron accumulation layer are presented. They were obtained from the electron density 20 nm below the Si-SiO_2 interface using as condition a value of the electron density equal to the bulk doping. Figure 5 left shows the results of a 2D-simulation for a sensor with 20 µm gap, 5 µm metal overhang and radiation effects corresponding to 1 MGy for a 500 µm thick sensor biased to 500 V.

The voltage dependence for different dose values is shown in the right plot of figure 5 for sensor with a 20 µm gap, 5 µm metal overhang and 1.2 µm junction depth. The difference between the gap width and the accumulation layer width is plotted, since the surface current is proportional to this difference. As can be seen, in the non-irradiated case a small (3.5 - 7.5 µm), only weakly voltage dependent accumulation layer is present. In the case of 100 kGy and 1 MGy at low voltages practically the entire region between the junctions is covered by the accumulation layer and for high voltages the region under the metal overhang depletes. For 10 MGy the breakdown voltage is 494 V, where as criterion for breakdown an electron or hole ionization integrals equals to one was used [12].

2012 JINST 7 C01006

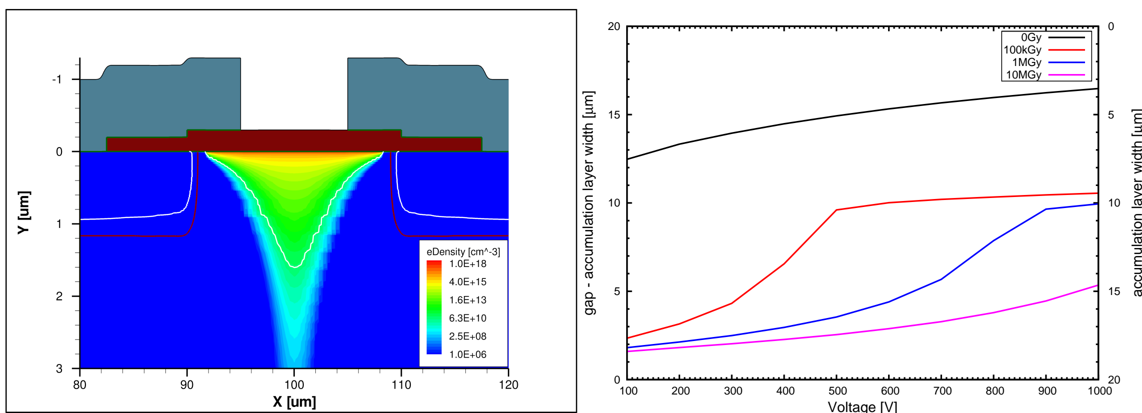

Figure 5. Left: electron density for a sensor with 20 µm gap and 5 µm metal overhang at 500V and 1MGy. Right: difference of the width of the gap minus the width of the accumulation layer vs. voltage. The scale on the right side gives the accumulation layer width.

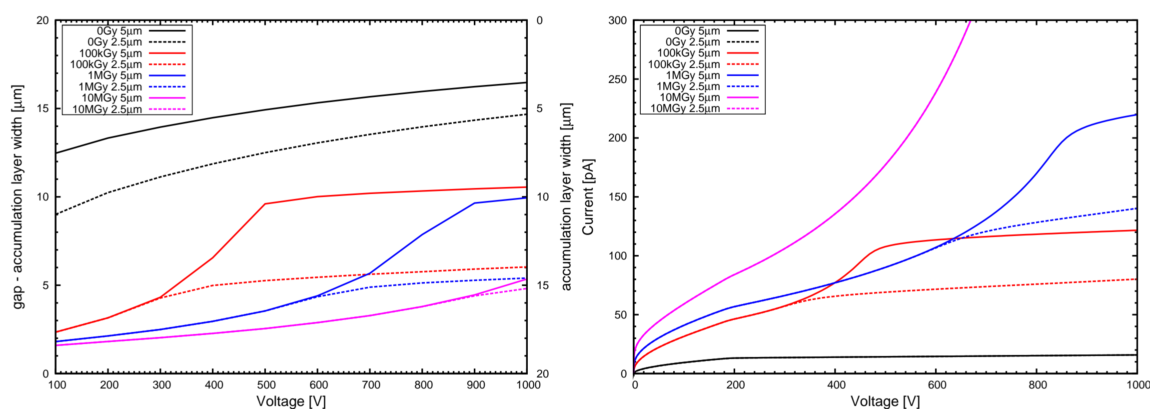

Figure 6. Left: difference of the width of the gap minus the width of the accumulation layer vs. voltage for a sensor with 2.5 and 5 µm metal overhang. Right: current vs. voltage for 2.5 and 5 µm metal overhang.

The effect of different overhang values, 2.5 and 5 µm, for the same gap and junction depth is shown in figure 6, where in addition to the difference gap-accumulation layer width the I-V curves are plotted. For irradiated sensors at sufficiently high voltages the accumulation layer for the 5 µm overhang is smaller than for the 2.5 µm resulting in a higher current for the larger overhang. In the 10 MGy case the breakdown voltage of 494 V is the same for both overhang values. Without metal overhang the breakdown voltage is much lower (296 V). The 20 µm gap is the smallest which was simulated. Therefore for all larger gap sizes the breakdown voltage will be lower.

The maximum electric field in the silicon for a given oxide thickness can only be reduced with a deeper junction, since this leads to a smaller curvature at the implant edges. For the 10 MGy and 20 µm gap, figure 7 shows the comparison of the maximum lateral electric field in the silicon as function of voltage for the 1.2 µm and 2.4 µm deep junctions. A reduction of the electric field is seen: at 500 V the electric field of the 2.4 µm deep junction is about 30% lower compared to the 1.2 µm junction. The breakdown voltage for the deep junction is in this case above 1000 V. Breakdown voltages above 1000 V were also obtained for a gap of 30 µm with 5 and 10 µm

2012 JINST 7 C01006

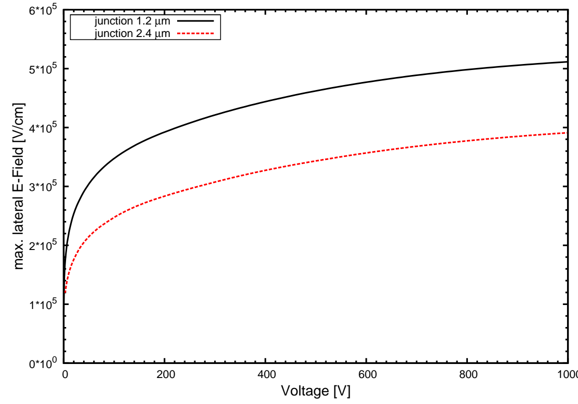

Figure 7. Maximum lateral electric field in silicon as function of voltage for sensors with a junction depth of 1.2 µm and 2.4 µm (20 µm gap, 5 µm overhang, 10 MGy).

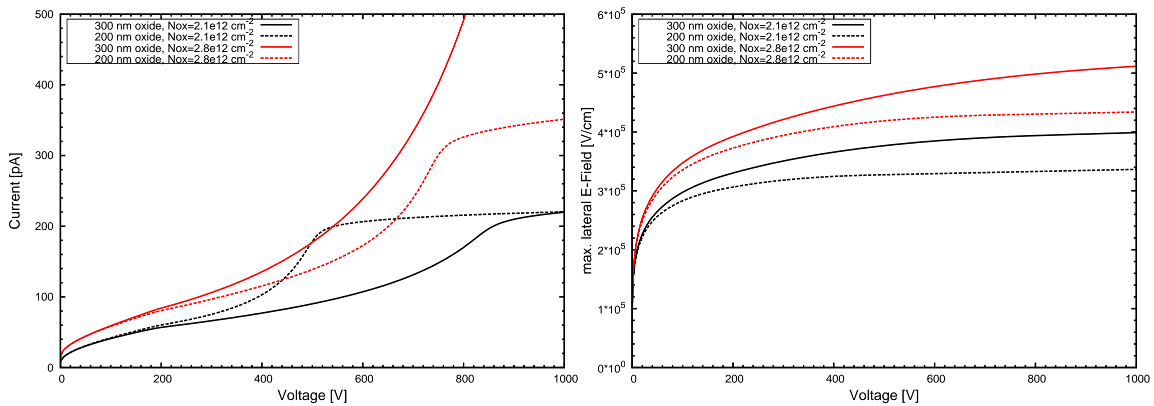

Figure 8. Left: current vs. voltage for a sensor with 200 nm and 300 nm thick oxide (20 µm gap, 5 µm overhang). Right: maximum lateral electric field in silicon as function of voltage for a sensor with 200 nm and 300 nm thick oxide. (20 µm gap, 5 µm overhang).

overhang and 40 µm gap with 10 µm overhang. From the I-V curves it is found, that the current of all investigated cases are within the specifications.

Another possibility to reduce the maximum electric field inside the silicon is the reduction of the oxide thickness as can be seen in the right plot of figure 8, where the maximum lateral electric field in the silicon as function of voltage for an oxide thickness of 200 and 300 nm is plotted. The simulations are again performed for the 20 µm gap, 5 µm overhang and the 1.2 µm deep junction. In addition the assumption was made, that the amount of fixed oxide charges are the same in both cases. A fixed oxide charge density of $N_{ox} = 2.1 \times 10^{12}$ cm^{-2} corresponds to a dose of 1 MGy and $N_{ox} = 2.8 \times 10^{12}$ cm^{-2} corresponds to a dose of 10 MGy for a 300 nm thick oxide.

The reduction of the field at 500 V is about 15% for the lower and about 8% for the higher oxide charge. From the I-V curves, left plot of figure 8, it can be seen, that for the thinner oxide the region under the metal overhang depletes at lower voltages and the breakdown is above 1000 V.

To compare the results of the 2D (strip) simulations with 3D (pixel) simulations a quarter of a pixel with a gap of 20 µm and 5 µm overhang was simulated. Due to difficulties in including the doping profile from the process simulation a Gaussian profile with a junction depth of 1.5 µm was

2012 JINST 7 C01006

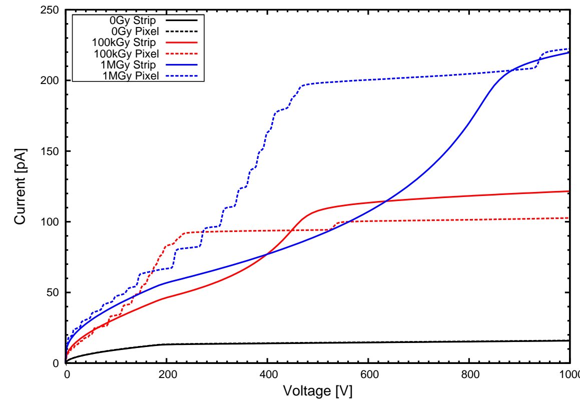

Figure 9. Comparison of the I-V characteristics between 2D (strip) and 3D (pixel) simulation for different dose values (20 µm gap, 5 µm overhang).

used. The number of mesh points was 4.4×10^5 and 9.5×10^5 for the 3D case, where approximately 80% of the grid points were used for the refinement of the mesh at the Si-SiO_2 interface. The total cpu time for the simulations using the smaller mesh were, depending on the dose, 180 h to 406 h.

In figure 9 the I-V curves for the smaller mesh for different dose values together with the results of the 2D simulations are shown. The steps in the I-V curves in the 3D simulations are related to the mesh of the Si-SiO_2 interface below the metal overhang. Using the finer mesh gives similar I-V curves, only the steps were reduced.

From the comparison of the I-V curves of the 2D and 3D simulations one finds, that for low and high voltages the simple scaling of the geometry gives reasonable results. In the 3D simulation however, the depletion under the metal overhang appears at a lower voltage, which causes the difference of the voltage dependence of the 2D and 3D simulated current.

To verify that the specification of the inter-pixel capacitance can be met with the simulated geometries, 2D capacitance simulations were performed. For all geometries and doses the full depletion voltage is in the range of 188-194 V and the capacitance of a pixel to the backplane is 8.5 fF. In table 4 the simulated inter-pixel capacitances for a junction depth of 1.2 µm and a overhang of 5 µm are given for a dose of 0 Gy and 1 MGy. The values for the capacitance are given at full depletion (190 V) and at 500 V. Since, the accumulation layer decreases with voltage also the inter-pixel capacitance decreases. The reason why at the depletion voltage the interstrip capacitance at 1 MGy for the 40 µm gap is larger then for the 30 µm gap, is still under study. All inter-pixel capacitances are well within the specifications (< 0.5 pF).

5 Summary

Using MOS capacitors and gate controlled diodes the oxide charge density, the density of interface traps and their properties were determined as function of dose up to 1 GGy. These dose dependent parameters were used in the TCAD simulation to predict and optimize the performance of sensors designed for the AGIPD project.

From the simulation it is found, that the specification of dark current, inter-pixel capacitance and full depletion voltage can be met.

2012 JINST 7 C01006

Table 4. Calculated inter-pixel capacitance for 1.2 μm deep junction and 5 μm overhang.

		V = 190 V			V = 500 V		
Gap μm	Dose MGy	acc. layer [μm]	2D C_{int} [fF/μm]	3D C_{int} [fF]	acc. layer [μm]	2D C_{int} [fF/μm]	3D C_{int} [fF]
20	0	6.7	0.12	96	5.1	0.12	93
	1	17.9	0.39	305	16.5	0.33	259
30	0	13.3	0.10	73	10.3	0.10	71
	1	26.8	0.17	117	20.1	0.13	92
40	0	19.8	0.09	59	15.4	0.09	56
	1	34.3	0.25	163	29.5	0.13	82

Acknowledgments

This work was done within the Project *Radiation Damage* financed by the European XFEL-Company in close collaboration with the AGIPD project. Additional support was provided by the Helmholtz Alliance *Physics at the Terascale*.

References

[1] M. Altarelli et al., *European X-ray free electron laser technical design report*, *Technical Report*, The European XFEL, (2007).

[2] H. Graafsma, *Requirements for and development of 2 dimensional X-ray detectors for the European X-ray Free Electron Laser in Hamburg*, 2009 *JINST* **4** P12011.

[3] J. Becker et al., *Impact of plasma effects on the performance of silicon sensors at an X-ray FEL*, *Nucl. Instrum. Meth.* **A 615** (2010) 230.

[4] A. Akkerman et al., *Updated NIEL calculations for estimating the damage induced by particles and gamma-rays in Si and GaAs*, *Radiat. Phys. Chem.* **62** (2001) 301.

[5] H.J. Barnaby, *Total-Ionizing-Dose Effects in Modern CMOS Technologies*, *IEEE Trans. Nucl. Sci.* **53** (2006) 3103.

[6] J. Zhang et al., *Study of radiation damage induced by 12 keV X-rays in MOS structures built on high resistivity n-type silicon*, arXiv:1107.5949.

[7] J. Zhang et al., *Study of X-ray Radiation Damage in Silicon Sensors*, *13th International Workshop on Radiation Imaging Detectors*, ETH Zurich Switzerland, July 3–7 2011, paper submitted.

[8] H. Perrey, *Jets at Low Q^2 at HERA and Radiation Damage Studies for Silicon Sensors for the XFEL*, Ph.D Thesis, Hamburg University, DESY-THESIS-2011-021 (2011) 153.

[9] B. Henrich et al., *The adaptive gain integrating pixel detector AGIPD, a detector for the European XFEL*, *Nucl. Instrum. Meth.* **A 633** (2011) S11.

[10] G. Potdevin et al., *Performance simulation of a detector for 4th generation photon sources: The AGIPD*, *Nucl. Instrum. Meth.* **A 607** (2009) 51.

[11] Synopsys TCAD, webpage http://www.synopsys.com.

2012 JINST 7 C01006

[12] S. Sze et al., *Physics of semiconductor devices*, John Wiley & Sons, Inc., Hoboken, New Jersey U.S.A. (2007).

[13] P. Cattaneo, *Capacitances in micro-strip detectors: A conformal mapping approach*, *Solid State Electron.* **54** (2010) 252.

[14] A. Cerdeira et al., *Analytical expressions for the calculation of pixel detector capacitances*, *IEEE Trans. Nucl. Sci.* **44** (1997) 63.

2012 JINST 7 C01006